

A Shielding System Proposal for the Cabling of Electric Glass Melters

ALDO CANOVA AND MICHELE QUERCIO 

Energy Department, Politecnico di Torino, 10129 Torino, Italia

CORRESPONDING AUTHOR: MICHELE QUERCIO (e-mail: michele.quercio@polito.it)

This work was developed by the IEEE Publication Technology Department. This work is distributed under the LaTeX Project Public License (LPPL) (<http://www.latex-project.org/>) version 1.3. A copy of the LPPL, version 1.3, is included in the base LaTeX documentation of all distributions of LaTeX released 2003/12/01 or later.

ABSTRACT This paper analyses the impact on workers of the electromagnetic field produced by large furnaces for glass production. The paper also propose a solution for the reduction and the containment of magnetic induction levels below the limits imposed by national and international directives. Using a three-dimensional numerical calculation code based on the hypothesis of filiform conductors in the air (Biot-savart law). The choice of the solution is based on the technique named highly coupled magnetically passive loop technique (HMCPL). The solution was then implemented and a comparison between the magnetic induction values before and after the installation of the shielding solution is presented.

INDEX TERMS Magnetic field pollution, shielding system.

I. INTRODUCTION

Existing research recognises the critical role played by the exposure of workers to electromagnetic fields [1]–[5]. At low frequency, the exposure to magnetic field has been shown to be related to adverse effects in circulation of currents within the body [6], [7]. The intensity of these currents depends on the intensity of the external magnetic field. If sufficiently high, these currents can cause damage of nerves and muscles or influence other biological processes. So far, very little attention has been paid to the role of low frequency magnetic field generated by the glass manufacturing furnaces. There is little published data on simulation of furnaces for glass production and directed mainly to the modeling of current temperature and flow fields inside the furnace [8]–[12]. The most complex simulation requires a three-dimensional CFD-type calculation code [13], [14] and one of the main open problems concerns the knowledge of the electrical characteristics of the glass as it varies in temperature and composition. Even just the resistivity depends on these parameters and it is not easy to find in literature closed formulas that provide this parameter. The magnetic field levels generated by the glass manufacturing furnaces are above the exposure threshold indicated by the regulatory bodies, the Institute of Electrical and Electronic Engineers (IEEE) [15], [16] and the International Commission

on Non Ionizing Radiation Protection (ICNIRP) [17]–[19], for this reason a shielding system must be applied to limit these levels. A possible solution is based on the use of magnetic field line deflection systems using passive shields in the form of plates that has been proposed and used [20]. But, this solution has some issues including the significant heating of the plates due to losses in the iron. In the present work, a technique based on highly magnetically coupled passive loops (HMCPL) was considered. This technique has been widely used in the shielding of the junction areas of high-voltage lines [21], [22]. The overall structure of the study takes the form of nine chapters, including: System description, Model for calculating magnetic fields, Operating principle of the HMCPL system, Mitigation system scheme, Syzed and preliminary analysis of the magnetic core, Results after shielding, Final layout of the system, Pre and Post shielding magnetic measurements, Conclusion.

II. SYSTEM DESCRIPTION

All electrically powered furnaces for glass production typically consist of a set of three pairs of electrodes. Each pair is made up of a set of opposed (eg 2-3 electrodes) and each triad is powered by a 50 Hz electric current of several

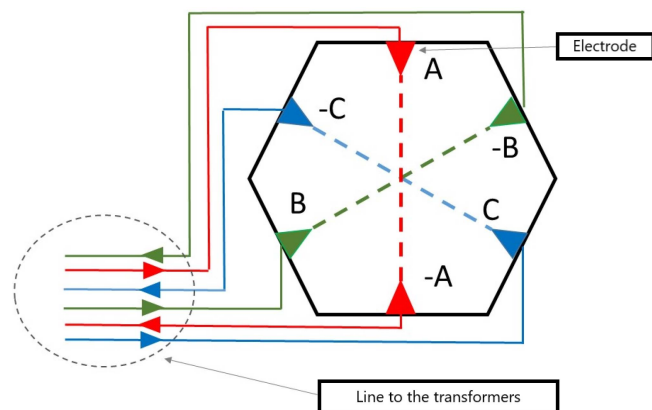


FIGURE 1. Circuit diagram of electric currents.

thousand amperes. The currents are produced by three single-phase transformers powered by a three-phase medium voltage transformer. The triad of currents that feed the electrodes is balanced (equal currents and 120 degrees out of phase). The electrical distribution is carried out by means of three single-phase lines (outward and return) that start from the transformer room and lead to the furnace. Distribution can be accomplished either by cables or by busbar lines. [23]. The currents entering the furnace generate an electrical neutral point inside the molten glass. In the furnace area, the forward and reverse currents move away from each other to reach the respective electrodes. This distancing of the conductors belonging to each phase results in a significant increase in magnetic fields (thousands of μT). The magnetic field generated between the furnace area (before each phase splits) and the transformers may be less critical, since the compensation given by the proximity between the forward and return currents of each phase can be better exploited [24]. There is therefore a need to reduce the magnetic field generated, both to protect inspection and maintenance workers in the vicinity of the furnace and to avoid induced currents in conductive components (e.g. metallic duct or structural metallic parts) near and around the furnace itself. At the beginning, the distribution of the conductors is as in Fig. 1 where the line towards the transformers and the distribution of the lines under the furnace are shown. The dotted lines indicate the path of the currents inside the furnace but this distribution is qualitative. This theoretical scheme of Fig. 1 is implemented in the real application as reported in Fig. 2, which shows the geometry of the busbar power lines indicating the closure of the currents inside the furnace. Mitigation of magnetic induction in the sections where the forward and return conductors diverge is particularly critical. In order to apply the HMCPL system to the case of the furnace with the use of busbar lines, it is necessary to foresee the presence of the conductors for the closing of the shielding loops already integrated inside the busbar lines themselves. In practice, in the two sections where there is only the outward or the return, the same busbar line used in the outward/return section is used. In this way it is possible to

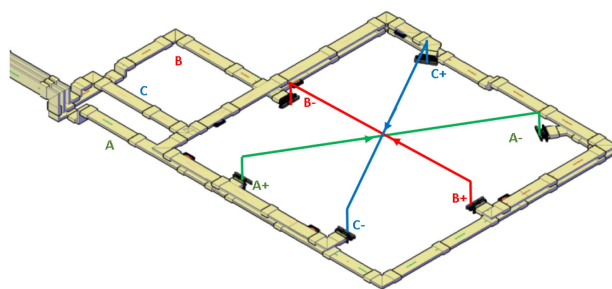


FIGURE 2. Geometric scheme of the distribution of the busbar power line close to the furnace.

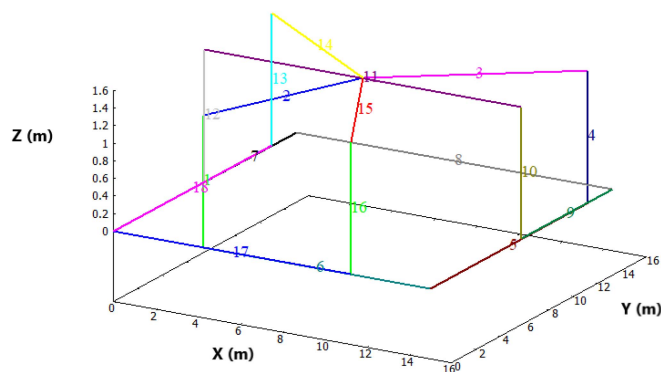


FIGURE 3. Filiform model of the electrical connections around the furnace and of the current inside the glass.

use the busbar that would be inactive to create the shielding loop. The work presented uses the nominal powers absorbed by the furnace without going into modeling the phenomena within it.

III. MODEL FOR CALCULATING MAGNETIC FIELDS

A circuit model was built based on the described furnace geometry.

- 1) Dimensions of total surface area hexagonal 44 m^2
- 2) Power 1.6 MW per phase / 4.8 MW total
- 3) Average melting temperature at $1400 \text{ }^\circ\text{C}$
- 4) Type of glass Named Soda Lime
- 5) Maximum glass yield 80 Tons / day.

The model calculates the contribution of the various conductors through the integral of the Biot-Savart formula [25]. Attention was focused on the sections of the line in the furnace area, leaving out the path between the transformers and the furnace, for the reasons indicated above (the section where the magnetic field is already contained). Fig. 3 shows the circuit model of the connections near the furnace according to the geometry. The filiform model represents a simplified approach but allows the evaluation of the magnetic induction values around the sources with good accuracy. The plane on which the conductors around the furnace are arranged is placed at the reference height $z = 0$. The height towards the electrodes was considered equal to 1.5 m.

A first level of interest is that:

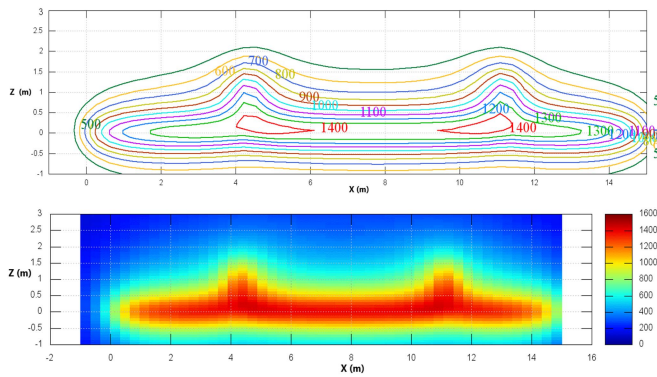


FIGURE 4. Isopleth lines and chromatic map of magnetic induction on a vertical plane close to the electrodes.

- XZ plane (X between -1 and 15 m, Z between -1 and 3 m) at 50 cm from the sources ($Y = -0.5$ m). It can be observed that there is a large area with an induction value greater than $1000 \mu T$.

Another area of interest is represented by the area under the furnace and Fig. 5 shows the level lines and the color map on the plane placed half a meter below the conductor plane:

- XY plane (X between -1 and 15 m, Y between -1 and 15 m) at $X = -0.5$ m

It is possible to observe that even in this area there is a wide range in which values above $1500 \mu T$ are reached.

IV. OPERATING PRINCIPLE OF THE HMCPL SYSTEM

The proposed system allows mitigating the magnetic field produced by a source, consisting of a set of conductors, through the second system of conductors, magnetically coupled to the source and suitably arranged in space. The conductors that carry out the mitigation can be chosen optimally in terms of number, position, cross section. They allow the shielding current to circulate in the conductors, these are connected to form circuits with closed paths. The mitigation of the magnetic field results, as in the case of passive conductive screens, from the superposition of the effects of the two systems. The proposed idea is to provide a passive screen with high coupling with the source, i.e. a shield consisting of a set of conductors suitably connected in which the currents in the screen are induced through a magnetic coupling obtained through a series of toroids of ferromagnetic material with high permeability, suitably sized and linking the sources. The system is presented in principle as in Fig. 6.

Each phase of the source links the magnetic core N_1 times ($N_1 = 1$ in the case of the figure); a winding of N_2 turns arranged on the core feeds the shield conductors. Through the magnetic core, a practically ideal magnetic coupling is made between the source circuit and the shield circuit. The presence, in the case under examination, of three phases requires that three shielding circuits be made. There are many variations of this solution, determined by the geometry of the source, by the choice of geometry, and by the N_1/N_2 ratio. The simplest configuration is the one in which $N_1 = 1$ and $N_2 = 1$

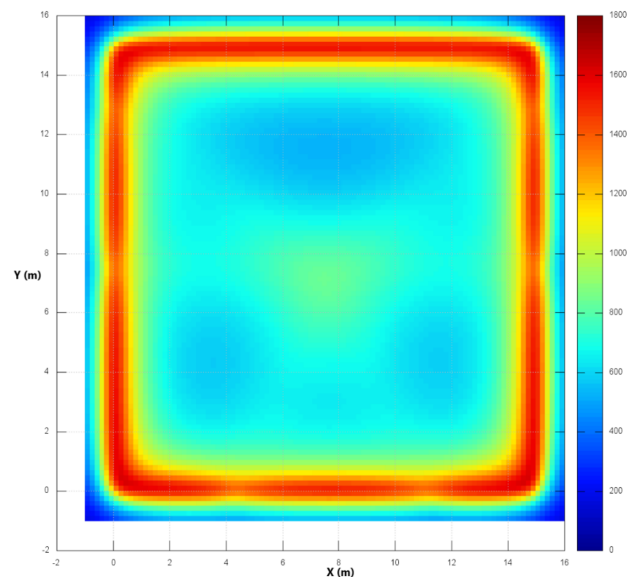
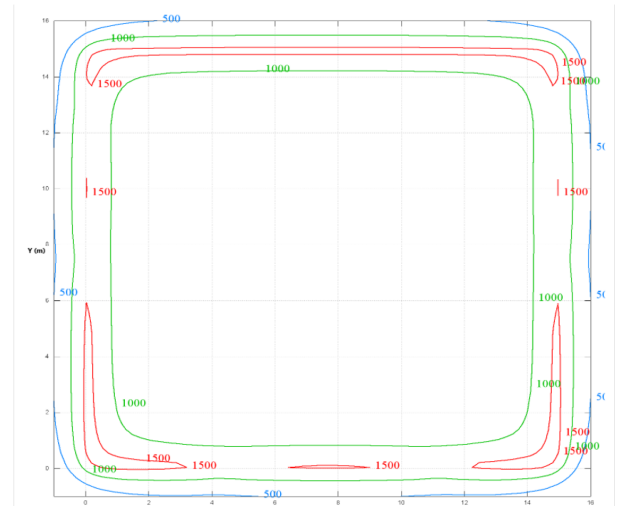


FIGURE 5. Isopleth lines and chromatic map of magnetic induction on a horizontal surface placed under the furnace.

(unity coupling). In this configuration, the coupling between the source and the shield is characterized by a unitary transformation ratio and the current in the shield and the source coincide [22]. One of the aspects that makes this shielding solution very efficient is that the two currents, are naturally in phase opposition. Referring to Fig. 7, which indicates the single-phase equivalent circuit of the coupling between the two circuits, in which:

- the source 1 is represented by the current generator I_1 ;
- the magnetic core 3 is represented by the transformer model.

For which Z_0 describes the losses in the iron and the magnetizing current, the transformation ratio describes the coupling between source 1 and screen 2. Resistance and inductive reactance of winding 4 are respectively described by R_T and X_T . Finally, I_{SH} , R_{SH} and X_{SH} represent the induced

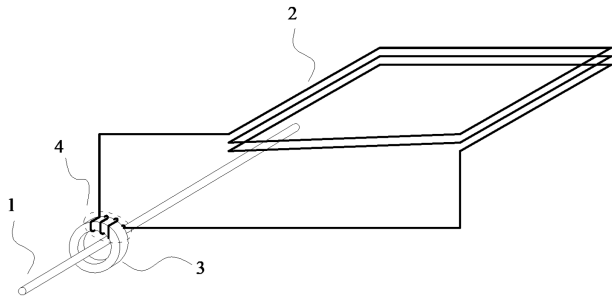


FIGURE 6. HMCPL shielding principle diagram: 1) source circuit, 2) shield circuit 3) coupling toroid, 4) shield circuit power winding.

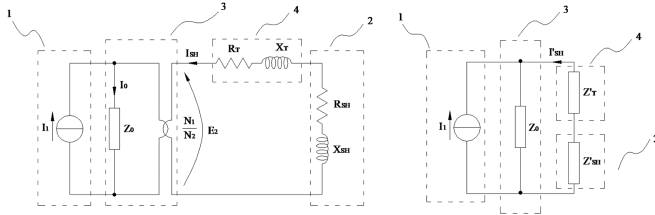


FIGURE 7. Circuit diagram of the HMCPL shield relating to a phase of the furnace power system.

current, resistance and inductive reactance of the shielding conductor 2.

With reference to Fig. 7, the currents are equal to:

$$I_{SH} = - \frac{E_2}{(R_T + R_{SH}) + j(X_T + X_{SH})} \quad (1)$$

$$I'_{SH} = - I_{SH} \frac{N_2}{N_1} \quad (2)$$

$$I_1 + I'_{SH} = I_0 \quad (3)$$

If the core is well sized, the current I_0 which includes losses in the iron and magnetizing current is negligible so it can be said that:

$$I_{SH} = - \frac{E_2}{(R_T + R_{SH}) + j(X_T + X_{SH})} \quad (4)$$

$$I'_{SH} = - I_{SH} \frac{N_2}{N_1} \quad (5)$$

$$I_1 \approx - I'_{SH} = I_{SH} \frac{N_2}{N_1} \quad (6)$$

Therefore, the current flowing through the conductors of shield 2 naturally results in phase opposition to the current of source 1. The design process is based on the sizing of the magnetic core and the choice of the cross-section of the screen conductors. In the application under study, the number of source and screen turns is unitary and therefore the maximum screen current is equal to the source current. The proposed system has significant advantages:

- 1) It is self-adaptive being a passive screen.
- 2) No screen power systems are required: it is the source itself that powers the screen through the magnetic core.

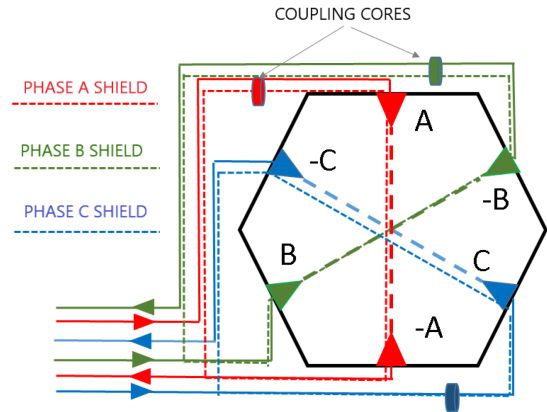


FIGURE 8. Principle diagram of the HMCPL shield applied to the distribution of the electrode supply lines.

- 3) Currents are much higher than in traditional passive screens (passive mesh screens or conductive flat screens).
- 4) The currents are naturally in phase opposition and therefore allow to obtain the maximum shielding effect as regards the phase.
- 5) The shielding factor of the proposed HMCPL system can reach values at least equal to 20 times.
- 6) It is possible to use, in the case of coupling with $N_2 = 1$, the same conductor used for the source with a considerable advantage from the point of view of supply.

V. MITIGATION SYSTEM SCHEME

The basic diagram of the shield loops is presented in Fig. 8. The shielding loop is made up partly of the busbar itself and in part of reclosing sections which can be in cable or, as in the case in question, by busbar ducts. The system, therefore, has three shielding loops, one for each phase. The screen conductors are therefore characterized by sides in which the coupling between source and screen is such as to allow an almost cancellation of the magnetic field. On the contrary, near the electrodes, the shielding loops will “come out” from the busbar duct and will close again by closing the loops. In this section, the same will cross the area under the furnace and the magnetic field compensation will be partial (currents in the loop and currents in the furnace). Greater geometric detail is shown in Fig. 9 where the closure scheme in shielding loops for the three phases is shown. The figure shows how the course of the paths is different from the theoretical one and hypothesized in the diagram of Fig. 8. This is due to the architectural constraints of the area under the furnace (supporting columns) and the real dimensions of the connections. The final paths are slightly different from the ideal ones and this will result in a slight variation in the magnetic induction levels.

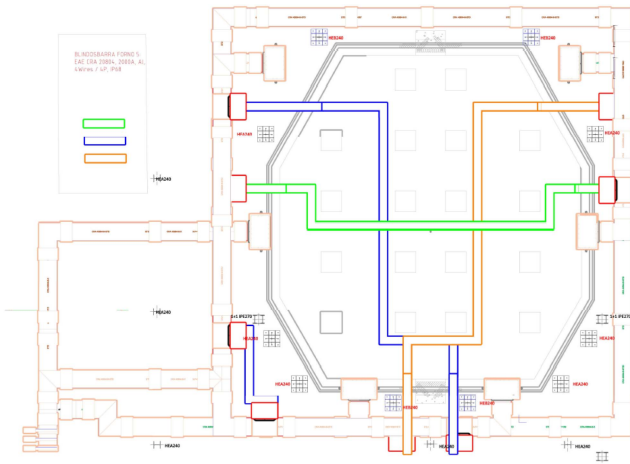


FIGURE 9. Scheme of the re-closing sections of the loops in the area under the furnace.

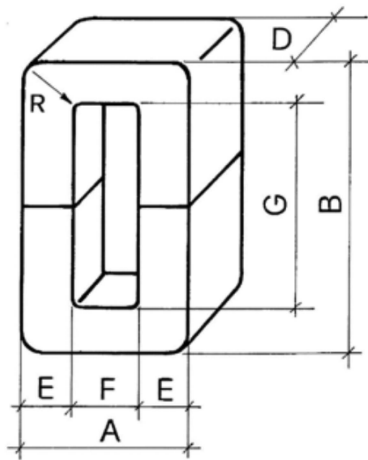


FIGURE 10. Diagram of the magnetic core of shield source coupling with indication of the dimensions.

VI. SIZING AND PRELIMINARY ANALYSIS OF THE MAGNETIC CORES

Based on the previous indications, three core prototypes with a cross-section of 20 cm² were created. The characteristics of the prototypes are shown in Fig. 10. The open-type core is therefore made up of two U-shaped half-parts which are held together by metal clamps. Two variants were analyzed: one of 40 mm × 50 mm and one of 20 mm × 100 mm. The closed core was made with the dimensions of variant 2. The dimensions in Fig. 11 refer to the diagram shown in Fig. 10.

A. COMPARISON BETWEEN CLOSED AND OPEN CORE

Magnetic measurements were made to compare the performance between closed and open core. The test consisted in magnetically exciting the core with a variable magnetization current until it reached saturation. From the value of the current it is possible to go back to the value of the magnetic field

| Parameter | Type 1 (open) | Type 2 (open) | Type 3 (closed) |
|-----------|---------------|---------------|-----------------|
| D (mm) | 50 | 100 | 100 |
| E (mm) | 40 | 20 | 20 |
| F (mm) | 110 | 110 | 110 |
| G (mm) | 600 | 600 | 600 |
| B=G+2*E | 680 | 640 | 640 |
| A=F+2*E | 190 | 150 | 150 |








FIGURE 11. Geometric dimensions of the two proposed variants.

H while from the value of the voltage induced on a secondary circuit it is possible to go back to the value of magnetic induction B through the relations:

$$H = \frac{N_1 I_1}{L} \quad (7)$$

$$B = \frac{V_2}{2\pi f S N_2} \quad (8)$$

where:

- N_1 : number of turns of the primary circuit (equal to 1) or excitation circuit;
- N_2 : number of turns of the secondary circuit (equal to 19) or flow detector circuit;
- L : length of the magnetic circuit (equal to: 1.52 m);
- f : net frequency (equal to 50 Hz);
- S : cross section of the magnetic circuit (equal to: 20 cm²);
- S : cross section of the magnetic circuit (equal to: 20 cm²);
- V_2 : induced voltage measured on the secondary;

The data obtained allow us to observe how the closed core has performances in terms of permeability higher than an order of magnitude compared to the open core. Figs. 12 and 13 show the trends of the magnetization curve and the equivalent relative permeability of the closed core and the open core.

VII. RESULTS AFTER SHIELDING

The shielding effect leads to an overall reduction in magnetic fields while maintaining relatively high local values in certain un-shielded areas. An example is the area near the electrodes as shown in Fig. 14 which shows the level lines and the chromatic map on the plane:

- XZ plane (X between -1 and 15 m, Z between -1 and 3 m) at 50 cm from the sources (Y = -0.5 m)

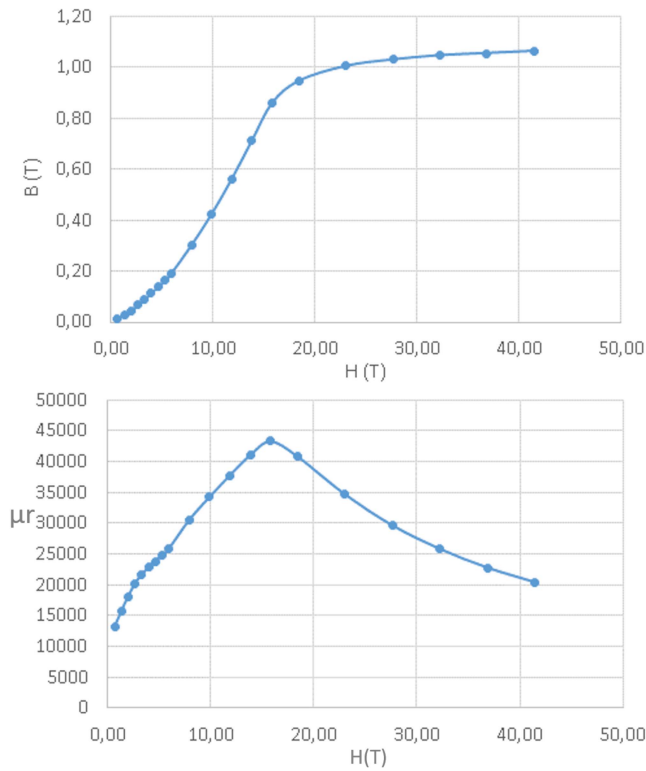


FIGURE 12. Magnetic characteristic and relative permeability of the closed core.

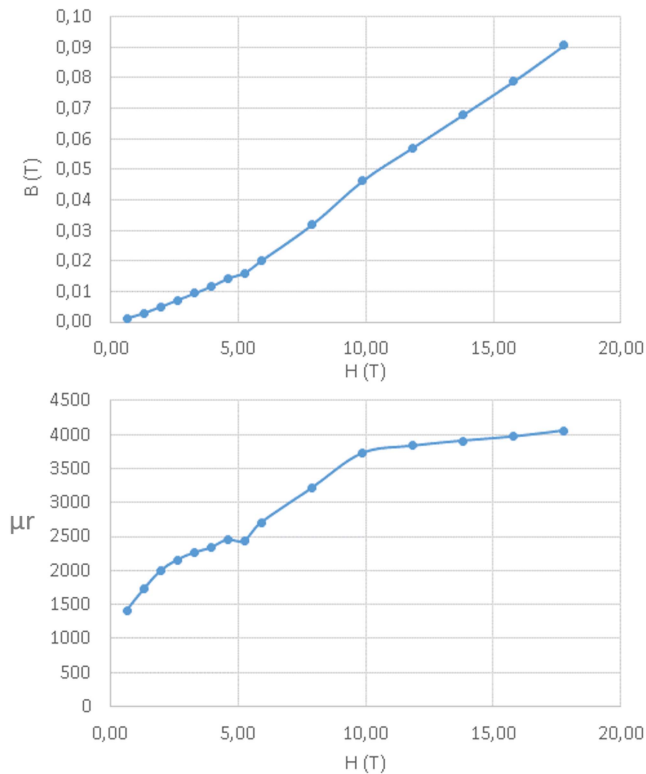


FIGURE 13. Magnetic characteristic and relative permeability of the open core.

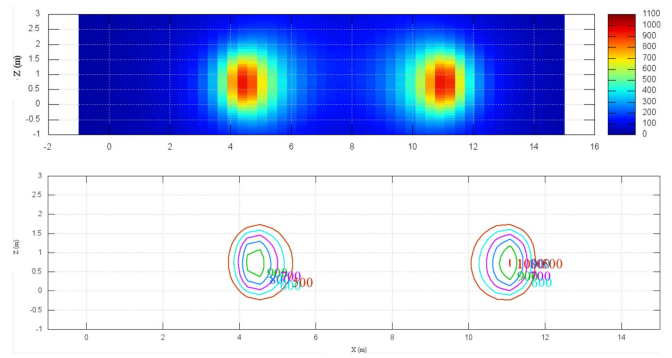


FIGURE 14. Level lines and chromatic map of magnetic induction on a vertical post-shielding plane.

The area under the furnace, where the shielding loops are closed, also has an interesting distribution of the post-shielding magnetic field. It can be observed that the entire area surrounding the furnace sees a significant reduction in the levels of magnetic induction but the presence of the re-closure connections of the shielding loops sees an increase in the magnetic field in the center of the surface under the furnace.

VIII. FINAL SIZING OF THE COUPLING CORES

As already reported in paragraph 5, the sizing of the core are linked to the voltage that the core must sustain in the loop circuit. This voltage can be considered equal to the voltage drop of the electrical line which is shielded and which runs parallel to the loop. The determination of this voltage drop cannot be carried out only by considering the service inductances of the busbars since the configuration of the connections under the furnace carries the single-phase current and not a three-phase current. The determination of the voltage drop can be estimated through analytical evaluations and verified with field measurements.

A. ESTIMATION OF THE INDUCTANCES OF THE LOOP CIRCUITS

This section presents the calculation of the inductance of the single-phase taking into account the loop that is formed between the closure of the loop and the current inside the furnace. Given the significant size of the loop that is formed, the inductance is particularly high. Inductance, therefore, represents the main term of the impedance of the secondary circuit seen from the magnetic core and this will result in a large number of cores.

B. VERIFICATIONS OF THE VOLTAGE DROPS

The measurement tools used to carry out this analysis were:

- Compact oscilloscope connected directly to the PC, of the 2-channel Pico Scope type.
- Differential probe for voltage detection.



FIGURE 15. Instrumentation connected to the electrodes: measurement of the current circulating in a single electrode.

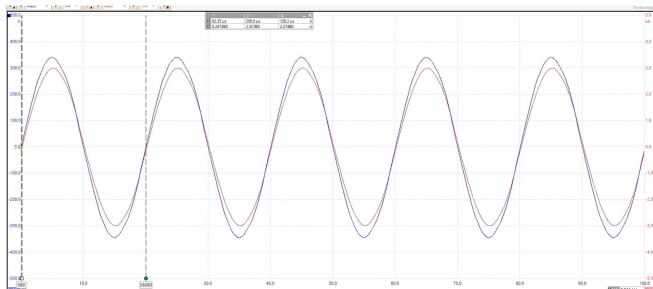


FIGURE 16. Phase "A" voltage and current supplied by the transformer.

- Rogowski type current probe, with direct signal processing.

The current present on one of the electrodes is defined as the reference quantity, and the RMS voltages coming out of the transformer and those arriving at the electrodes have therefore been measured. This indication allows defining the drop ΔV on the power supply circuit. The measurement of the voltage value at the output of the transformer was taken from a junction box containing three pairs of circuits connected directly to the LV terminals of the three transformers. The measurement of the voltage value present at the electrodes was detected by standing directly on an electrode on one side of the oven and reporting, via a dedicated cable, the opposite electrode. Measurements were made on each stage. Fig. 15 shows the area of the electrodes where the quantities of voltage and current and the instrumentation used were detected. The number of electrodes of each phase is equal to 3 but can also be less.

1) PHASE A

Phase "A" powers the furnace through 2 electrodes out of 3 and the current value detected is that relating to the single electrode. By way of example Figs. 16 and 17 shows respectively the voltage and current at the transformer terminals and

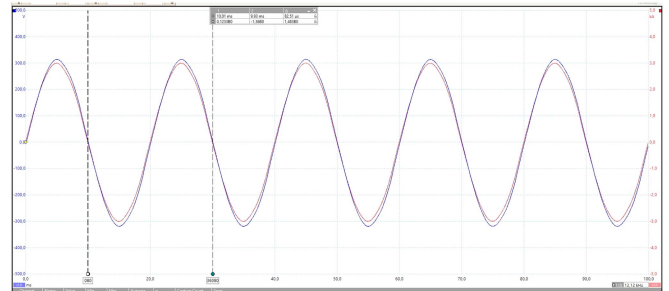


FIGURE 17. Phase "A" voltage and current measured at the electrodes.

the voltage and current at the electrodes. From the difference between the two voltage trends it is possible to derive the voltage drop.

- Voltage supplied by transformer "A": 240.7 V
- Electrode voltage: 222.4 V
- Current on one electrode: 2.10 kA
- $\Delta V = 18.3$ V

2) PHASE B

Phase "B" powers the furnace through 3 electrodes out of 3 and the current value measured is that of a single (central) electrode. The measured data are:

- Voltage supplied by transformer "B": 230.0 V
- Electrode voltage: 216.0 V
- Current on one electrode: 1.36 kA
- $\Delta V = 14$ V

3) PHASE C

Phase "C" powers the furnace through 2 electrodes out of 3 and the current value measured is that of a single electrode. The measured data are:

- Voltage supplied by transformer "C": 238.8 V
- Electrode voltage: 229.6 V
- Current on one electrode: 2.20 kA
- $\Delta V = 9.2$ V

From the results obtained it can be observed that the voltage drop varies between 9 and 18 V. This value is slightly greater than the voltage drop that must be sustained by the cores as it is necessary to take into account two aspects:

- There will be a "natural" coupling due to the proximity of the shield circuit with the source circuit in the sections in which the two circuits are made up of the busway;
- Part of the voltage drop is in the section between the transformers and the area in which the round trip moves away (area to be shielded) and therefore external to the shield.

Therefore, assuming a working induction not exceeding 1 T, a maximum voltage equal to 18 V and a cross section of the core equal to 30 cm², the number of cores to be installed on each phase is equal to:

$$N = \frac{V}{2\pi fSB} \simeq 19 \quad (9)$$

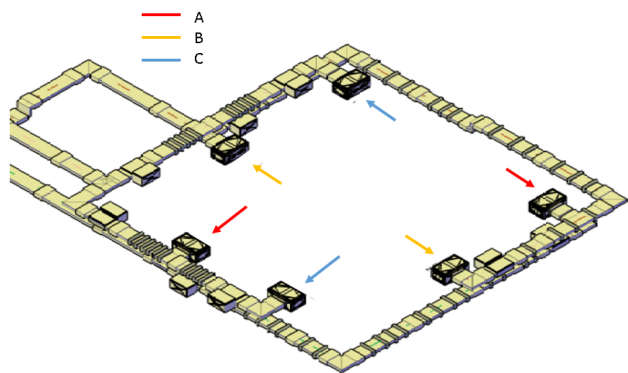


FIGURE 18. Distribution of the coupling cores on the different phases.

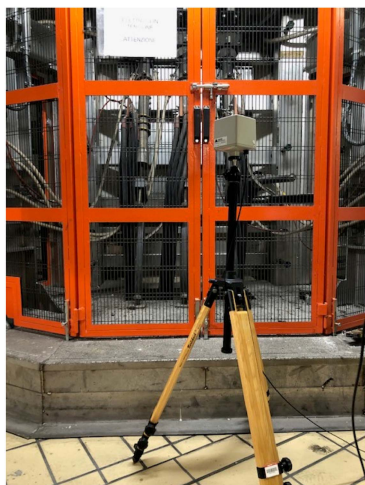


FIGURE 19. Measurement point in front of electrodes.

IX. FINAL LAYOUT: CLOSING OF THE SHIELDING LOOPS AND POSITIONING OF THE COUPLING CORES

The relatively large number of magnetic cores to be placed on each phase is distributed along the busbar according to the layout shown in Fig. 18 relative to phases A, B, and C. In phases, A and B 20 cores were distributed, with a maximum of 3-4 cores for each section of approximately 3 m. In phase C, characterized by a length available for the installation of the lower cores, it is possible to insert 18 cores. The slightly lower number leads to a slightly higher induction of work in the core. Fig. 18 also shows the trend of the closing paths of the shielding loops made using busbars.

X. PRE AND POST SHIELDING MAGNETIC INDUCTION MEASUREMENTS

A. FURNACE AREA: GROUND FLOOR

The area surrounding the furnace on the ground floor was subject to magnetic field measurements at the points considered significant: in front of the electrodes (Fig. 19) and front of the furnace between the electrodes (Fig. 20). Taking into account that the main contribution to the magnetic field comes from the electrodes themselves and the power distribution of the electrodes placed on the pit floor, the measurement was



FIGURE 20. Measurement point between electrodes.

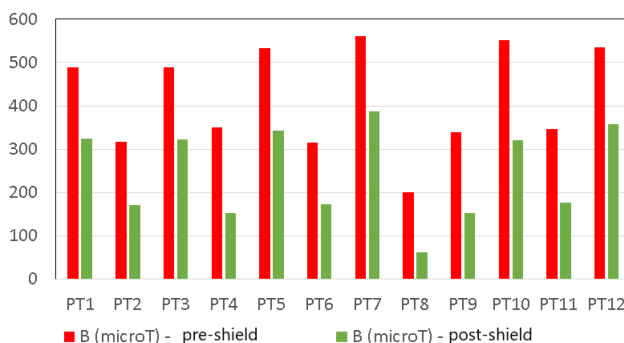


FIGURE 21. Measured magnetic induction on the ground floor before and after the shielding installation.

carried out at an altitude of 1 m from the walking surface. Fig. 21 shows the magnetic flux density before and after the shielding installation. It can be observed that the shielding has a significant effect of reducing exposure even on the ground floor.

B. FURNACE AREA: AREA NEXT TO THE BUSBARS

The area surrounding the so-called pit floor is an area of great interest as the one closest to the busbar that was the subject of the mitigation intervention. Measurements were made in various points considered significant and reported in the diagram of Fig. 22.

The measuring points are characterized according to the indications of Fig. 26, which also reports the pre and post-closing values of the shielding loops. The points analyzed are placed at an altitude of 1.5 m from the walking surface and can be traced back to two main groups: points that are most affected by the shielding effect and points that are affected by the effect of un-shielded sections (highlighted in blue). The

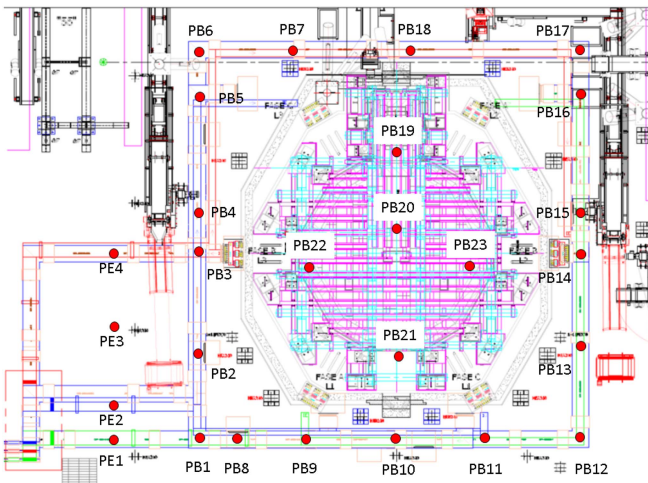


FIGURE 22. Indication of measurement points in the pit area.



FIGURE 23. Sections of the closure of loops A and C: a) path under the furnace; b) ascent towards the busbar ducts.



FIGURE 24. Electrode power cables.

former has a significant reduction in the magnetic field that can even reach 10 times (eg PB13 and PB14); the latter is still affected by the effect of unshielded sources: the departures of the shielding loop closures (Fig. 23) or the power cables of the electrodes of the three phases A, B, and C (Fig. 24). In these points, the reduction of the magnetic field due to

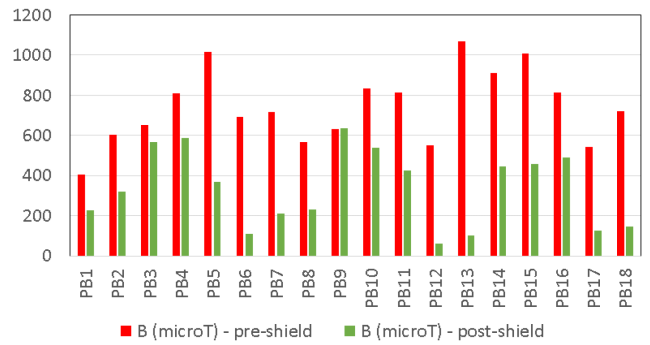


FIGURE 25. Measured magnetic induction before and after the shielding installation in the pit area.

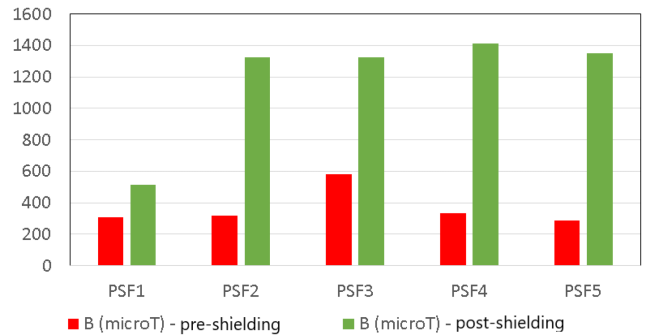


FIGURE 26. Measured magnetic induction before and after the shielding installation in the area under the furnace.

the shielding is less significant and is around 1.5-2 times. To provide a graphic overview, Fig. 25 shows the contribution of the shielding system to the magnetic field reduction.

The presence of the closing sections of the shielding loops naturally generates magnetic induction values significantly higher than the previous values in the sub-furnace area (as shown in Fig. 26). This area is normally forbidden to workers but in the case of access to this area, exceeding the lower action value (1000 microT) leads to the request of one of the following solutions:

- limit access to this area only to workers classified as “professionally exposed”;
- assessment of exposure levels (dosimetric calculations) in order to evaluate the conformity of the area even for workers who are not professionally exposed: it is possible, in fact, that dosimetric calculations do not need to classify the area as exclusive access to professionally exposed workers;
- install in correspondence with some points of the “shielding barriers” operating according to the principle of “flux shunting” that limit the magnetic induction values in access areas;

XI. CONCLUSION

This paper presented the highly coupled magnetically passive loop (HMCPL) system applied to the electrical circuit of a glass manufacturing furnace. This solution has been shown to

reduce the magnetic field values dangerous to workers. One of the advantages of this passive shielding is that it is self-adaptive since the shielding currents follow the time variation of the source. In addition, it does not require a shield power system since it is self-powered by the coupling system. The shielding currents are increased through a strong magnetic coupling with the sources that are obtained by means of appropriate magnetic cores. Closed magnetic cores minimize the magnetization current and maximize the coupling factor. The HMCPL is safe to shield cables in the junction area and it is also a suitable solution in order to shield the area near a glass manufacturing furnace.

ACKNOWLEDGMENT

The authors would like to thank Bormioli Luigi SpA (Parma) and to BESHielding SRL (Rivoli-Turin) for their willingness to publish the results. The opinions expressed here are entirely that of the author. No warranty is expressed or implied. User assumes all risk.

REFERENCES

- [1] M. Hosseini *et al.*, "Investigating the role of internal layout of magnetic field-generating equipment on workers' exposure at power substations," *Int. J. Occup. Saf. Ergonom.*, vol. 27, no. 1, pp. 1–7, 2021, doi: [10.1080/10803548.2018.1475927](https://doi.org/10.1080/10803548.2018.1475927).
- [2] A. Canova, F. Freschi, and M. Repetto, "Evaluation of workers exposure to magnetic fields," *Eur. Phys. J.-Appl. Phys.*, vol. 52, no. 2, 2010, Art. no. 23311.
- [3] A. C. Gubernati, F. Freschi, L. Giaccone, R. Scorretti, L. Seppecher, and G. Vial, "Modeling of exposure to low-frequency electromagnetic fields of workers in arbitrary posture," *IEEE Trans. Magn.*, vol. 56, no. 2, pp. 1–4, Feb. 2020.
- [4] G. Betta, D. Capriglione, and N. Pasquino, "Experimental investigation on workers' exposure to electromagnetic fields in proximity of magnetic resonance imaging systems," *Meas. J. Int. Meas. Confederation*, vol. 45, no. 2, pp. 199–206, 2012.
- [5] P. Gajšek, P. Ravazzani, J. Grellier, T. Samaras, J. Bakos, and G. Thuróczy, "Review of studies concerning electromagnetic field (EMF) exposure assessment in Europe: Low frequency fields (50 Hz–100 kHz)," *Int. J. Environ. Res. Public Health*, vol. 13, 2016, Art. no. 875. [Online]. Available: <https://doi.org/10.3390/ijerph13090875>
- [6] I. Magne and F. Deschamps, "Electric field induced in the human body by uniform 50 Hz electric or magnetic fields: Bibliography analysis and method for conservatively deriving measurable limits," *J. Radiological Protection*, vol. 36, no. 3, pp. 419–436, 2016, doi: [10.1088/0952-4746/36/3/419](https://doi.org/10.1088/0952-4746/36/3/419).
- [7] R. Kavet, M. A. Stuchly, W. H. Bailey, and T. D. Bracken, "Evaluation of biological effects, dosimetric models, and exposure assessment related to ELF electric- and magnetic-field guidelines," *Appl. Occup. Environ. Hyg.*, vol. 16, no. 12, pp. 1118–1138, 2001, doi: [10.1080/10473220127412](https://doi.org/10.1080/10473220127412).
- [8] A. A. Ghandakly and R. L. Curran, "Accurate modeling of interelectrode resistance and power dissipation in electric glass melters," *IEEE Trans. Ind. Appl.*, vol. 24, no. 6, pp. 1057–1061, Nov.-Dec. 1988.
- [9] S. Senan, U. Luedtke, and B. Halbedel, "Improving residence time distribution in glass melting tanks using additionally generated Lorentz forces," *J. Chem. Chem. Eng.*, vol. 9, pp. 203–210, 2015.
- [10] S. Laurent *et al.*, "A finite element modelling tool of a buried system for glass furnace wall characterization," *Eur. Phys. J. Appl. Phys.*, vol. 39, pp. 179–183, 2007.
- [11] A. Ungan and R. Viskanta, "Three-dimensional numerical simulation of circulation and heat transfer in an electrically boosted glass melting tank," *IEEE Trans. Ind. Appl.*, vol. IA/22, no. 5, pp. 922–933, Sep. 1986.
- [12] F. K. Choudhary, "Recent advances in mathematical modeling of flow and heat transfer phenomena in glass furnaces," *J. Amer. Ceram. Soc.*, vol. 85, no. 5, pp. 1030–1036, 2002.
- [13] C. Cravero and D. Domenico, "The use of CFD for the design and development of innovative configurations in regenerative glass production furnaces," *Energies*, vol. 12, 2019, Art. no. 2455, <https://doi.org/10.3390/en12132455>
- [14] A. F. J. A. Habraken *et al.*, "Glass melt quality optimization by CFD simulations and laboratory experiments," in *Proc. 76th Conf. Glass Problems*, 2016, pp. 169–77.
- [15] *IEEE Standard for Safety Levels With Respect to Human Exposure to Electromagnetic Fields, 0-3kHz.*, IEEE Standard C95.6.
- [16] *IEEE Standard for Safety Levels with Respect to Human Exposure to Radio Frequency Electromagnetic Fields, 3 kHz to 300 GHz.*, IEEE Standard IC95.1.
- [17] A. Ahlbom *et al.*, "Guidelines for limiting exposure to time varying electric, magnetic and electromagnetic fields (up to 300 GHz)," *Health Phys.*, vol. 74, no. 4, pp. 494–522, 1998.
- [18] ICNIRP, "Guidance on determining compliance of exposure to pulsed and complex non-sinusoidal waveform below 100 kHz with ICNIRP guidelines," *Health Phys.*, vol. 84, no. 3, pp. 383–387, 2003.
- [19] ICNIRP, "Guidelines for limiting exposure to time-varying electric and magnetic fields (1 Hz to 100 kHz)," *Health Phys.*, vol. 99, no. 6, pp. 818–836, 2010.
- [20] A. Canova, "Magnetic shielding of power supply of electrical glass oven," in *Proc. Int. Conf. Electricity Distrib.*, 2019, Art. no. 1732.
- [21] P. Ribaldone *et al.*, *On the Use of the HMCPL Shielding System in Renewing the Underground HV Power Lines in Big Cities*. Paris, France: CIGRE, 2016.
- [22] A. Canova *et al.*, "Magnetic shielding solutions for the junction zone of high voltage underground power lines," *Electric Power Syst. Res.*, vol. 89, pp. 109–115, 2012.
- [23] A. Ghandakly and R. L. Curran, "A model to predict current distributions in bundled cables for electric glass melters," *IEEE Trans. Ind. Appl.* vol. 26, no. 6, pp. 1043–048, Nov./Dec. 1990.
- [24] J. C. Bravo-Rodríguez, J. C. del-Pino-López, and P. Cruz-Romero, "A survey on optimization techniques applied to magnetic field mitigation in power systems," *Energies*, vol. 12, 2019, Art. no. 1332. [Online]. Available: <https://doi.org/10.3390/en12071332>
- [25] MAGIC Software: MAGnetic induction calculation. [Online]. Available: <http://www.satishielding.com/products-and-solutions/software-magic/>